Journal of Power Sources 263 (2014) 7–12

Contents lists available at ScienceDirect

Journal of Power Sources

journal homepage: www.elsevier.com/locate/jpowsour

High-energy X-ray powder diffraction and atomic-pair distribution-function studies of charged/discharged structures in carbon-hybridized Li_2MnSiO_4 nanoparticles as a cathode material for lithium-ion batteries

Maki Moriya [a], Masahiko Miyahara [a,*], Mana Hokazono [a], Hirokazu Sasaki [a], Atsushi Nemoto [a], Shingo Katayama [a,*], Yuji Akimoto [a], Shin-ichi Hirano [a,1], Yang Ren [b]

[a] Shoei Chemical Inc., 2-9-3 Suehiro, Ohme, Tokyo 198-0025, Japan
[b] X-ray Science Division, Argonne National Laboratory, 9700 South Cass Avenue, Argonne, IL 60439, USA

HIGHLIGHTS

- The carbon-hybridized Li_2MnSiO_4 nanostructured powders show the stable cycling performance with a capacity of ~190 mAh g^{-1}.
- HE-XRD and PDF analyses were carried out to study the discharged/charged structures.
- A long-range ordered structure dissipates in the discharged samples but each discharging process recovers it.
- The disappearance of the long-range order is caused by a local structure accommodating distortions of the MnO_4 tetrahedra.

ARTICLE INFO

Article history:
Received 17 December 2013
Received in revised form
11 March 2014
Accepted 17 March 2014
Available online 13 April 2014

Keywords:
Li_2MnSiO_4
Carbon-hybridized Li_2MnSiO_4 nanoparticles
Lithium ion battery
Cathode materials
High-energy X-ray powder diffraction
Atomic pair distribution function

ABSTRACT

The stable cycling performance with a high discharge capacity of ~190 mAh g^{-1} in a carbon-hybridized Li_2MnSiO_4 nanostructured powder has prompted an experimental investigation of the charged/discharged structures using synchrotron-based and laboratory-based X-rays and atomic-pair distribution-function (PDF) analyses. A novel method of in-situ spray pyrolysis of a precursor solution with glucose as a carbon source enabled the successful synthesis of the carbon-hybridized Li_2MnSiO_4 nanoparticles. The XRD patters of the discharged (lithiated) samples exhibit a long-range ordered structure characteristic of the (β) Li_2MnSiO_4 crystalline phase (space group $Pmn2_1$) which dissipates in the charged (delithiated) samples. However, upon discharging the long-range ordered structure recovers in each cycle. The disordered structure, according to the PDF analysis, is mainly due to local distortions of the MnO_4 tetrahedra which show a mean Mn–O nearest neighbor distance shorter than that of the long-range ordered phase. These results corroborate the notion of the smaller Mn^{3+}/Mn^{4+} ionic radii in the Li extracted phase versus the larger Mn^{2+} ionic radius in Li inserted phase. Thus Li extraction/insertion drives the fluctuation between the disordered and the long-range ordered structures.

1. Introduction

Polyanionic oxides such as $LiMPO_4$ phosphates and Li_2MSiO_4 silicates, (M = Fe, Mn), have been considered as promising cathode materials for rechargeable lithium ion batteries because of their better safety characteristics compared with those of the widely used cathode oxides such as $LiCoO_2$, $LiNiO_2$, and $LiMn_2O_4$. While such conventional cathode oxides undergone excessive delithiation result in activated oxygen release from the oxide lattice, polyanionic oxides do not have this problem. It has been considered that the activated oxygen acts as a strong oxidizer toward organic electrolytes.

Among polyanionic oxides lithium transition-metal orthosilicates Li_2MSiO_4 (M = Mn, Fe) have a theoretical capacity as high as 330 mAh g^{-1} owing to a dual electron transfer in $M^{2+}/M^{3+}/M^{4+}$ via extraction/insertion of two lithium ions in one formula unit [1]. Hence the structure and electrochemical performance of Li_2MSiO_4

* Corresponding authors.
E-mail addresses: m-miyahara@shoeichem.co.jp (M. Miyahara), shingok@rondo.plala.or.jp (S. Katayama).
[1] Shanghai Jiao Tong University, 800 Dongchuan Rd., 200240 Shanghai, China.

http://dx.doi.org/10.1016/j.jpowsour.2014.03.065
0378-7753/

have been investigated both experimentally and computationally [1–6]. Lithium iron orthosilicate Li_2FeSiO_4 is known to exhibit a stable cycling performance in the delithiation up to 1.0 Li/formula-unit which corresponds to the capacity of 165 mAh g^{-1} [7–25]. Recently, it was reported that the improved performance of Li_2FeSiO_4 was in the delithiation over 1.0 Li/formula-unit [26]. Lithium manganese orthosilicate Li_2MnSiO_4, on the other hand, shows a serious decrease in capacity upon cycling even though it has higher voltage than Li_2FeSiO_4 [1,5,27–55]. This decrease of capacity in Li_2MnSiO_4 has been attributed to the destruction of the crystal structure by a Jahn-Teller distortion associated with the Mn^{3+} ions [27].

We have synthesized a novel hybrid of carbon and Li_2MnSiO_4 nanoparticles that exhibit a stable cycling performance with a high discharge capacity of 190–205 mAh g^{-1}, corresponding to delithiation/lithiation of 1.15–1.24 Li/formula-unit [56]. The synthesis was achieved by in-situ carbonization of the Li_2MnSiO_4 nanoparticles with spray pyrolysis of a precursor solution with glucose as a carbon source. The stable cycling performance of the carbon-hybridized Li_2MnSiO_4 nanoparticles may be rationalized by the easy relaxation of structural distortions during delithiation/lithiation occurring only in extremely small particles of the order of 10 nm in diameter. However, the discharged/charged structures in the carbon-hybridized Li_2MnSiO_4 nanoparticles during cycling have not yet been determined.

In the present work, we have applied high-energy X-ray powder diffraction (HE-XRD) and atomic pair distribution function (PDF) analyses to study the discharged/charged structures in the carbon-hybridized Li_2MnSiO_4 nanoparticles that were in-situ synthesized by spray pyrolysis of a precursor solution with glucose as a carbon source.

2. Experimental

The carbon-hybridized Li_2MnSiO_4 nanoparticles were synthesized by spray pyrolysis followed by grinding and heat-treatment. The precursor solution for the spray pyrolysis was prepared by dissolving commercially available $LiNO_3$ (KANTO CHEMICAL CO., INC.), $Mn(NO_3)_2 \cdot 6H_2O$ (KANTO CHEMICAL CO., INC.), and colloidal silica (Nissan Chemical Industries, Ltd., SNOWTEX-OXS, colloid particle size: 4–6 nm, 10 wt% aq.) in distilled water in a stoichiometric ratio of Li_2MnSiO_4. The concentration of the elements in the precursor solution was 0.3 mol dm^{-3}. Further, glucose (Gun Ei Chemical Industry Co., Ltd.) was added into the precursor solution in a concentration of 100 g dm^{-3} (0.55 mol dm^{-3}) to provide the desired carbon content in the hybridized Li_2MnSiO_4 nanoparticles. The precursor solution was atomized by using an ultrasonic atomizer. The atomized mist of the precursor solution was introduced into a tube furnace (60 mmϕ, 850 mmL) heated at 600 °C by N_2 carrier gas (10 L min^{-1}), yielding a spray-pyrolyzed powder. Here, glucose was carbonized to form an amorphous carbon phase with the formation of Li_2MnSiO_4 phase. The spray-pyrolyzed powder was wetly grounded by high-energy ball-milling with 200 rpm for 270 min. The grounded powder was then heat-treated at 700 °C for 2 h in a flow of 1%H_2/Ar, producing carbon-hybridized Li_2MnSiO_4 nanoparticles with a carbon content of 12 wt%.

The carbon content in the carbon-hybridized Li_2MnSiO_4 nanoparticles was measured by a carbon/sulfur combustion analyzer (Horiba, EMIA-320 V).

The laboratory-based X-ray powder diffraction (XRD) experiments were performed by an X-ray diffractometer (Rigaku, RINT Ultima II with D/teX Ultra) with Cu Kα radiation.

The synchrotron-based XRD experiment was carried out on beam line 11-ID-C of the Advanced Photon Source, Argonne National Laboratory. The synchrotron X-ray energy was 115 keV (Wavelength: 0.1078 Å). A Laue Si(311) monochromator, thermally controlled to within 1.8° was used to provide the monochromatic X-ray beam. All samples were sealed in capillary tubes and the diffraction data were collected using a 2D X-ray area detector in transmission geometry.

The electrochemical characterization of the carbon-hybridized Li_2MnSiO_4 nanoparticles as a cathode material was performed using CR2032-typed coin cells at 25 °C. The composite cathode was prepared by mixing 20 mg of the carbon-hybridized Li_2MnSiO_4 nanoparticles and 15 mg of conductive binder (Teflonized acetylene black, TAB). The mixture was then pressed into an SUS-mesh which served as the current collector. The prepared electrodes were dried at 180 °C for 12 h in a vacuum oven. The coin cell was made up of a cathode and lithium metal sheet as anode, which were separated by a glass-wool sheet. The cells were filled with an electrolyte of 1 M $LiPF_6$ in a mixture of ethylene carbonate:dimethylene carbonate (1:2 ratio by volume), purchased from KISHIDA CHEMICAL Co., Ltd. The cells were galvanostatically charged up to 5.0 V in a limited charge of 206 mAh g^{-1} (a delithiation of 1.25 Li/formula-unit) and discharged down to 1.0 V on an electrochemical test instrument (NAGANO Co., Ltd., BT2010W). The charge/discharge rate was kept as 0.1 C in each cell. In order to avoid the effect of the degradation in cell parts other than Li_2MnSiO_4 during the charge/discharge cycles, some parts of a coin cell were periodically replaced by new ones at intervals of 20 cycles.

3. Results and discussion

Fig. 1 shows the charge/discharge profiles of the carbon-hybridized Li_2MnSiO_4 particles under the delithiation of 1.25 Li/formula-unit during the first five cycles. The profiles throughout the 2nd to the 5th cycles show the same behavior characteristic of a large discharge capacity of about 190 mAh g^{-1} (corresponding to lithiation about 1.15 Li/formula-unit) and a very high coulomb efficiency. Furthermore, succeeding cycling measurements confirmed the sustained stable charge/discharge profiles throughout until the 59th cycle. Only the first charge/discharge curves exhibit outstanding difference from all the other curves. Specifically, the potential of the first charge/discharge was higher than those of the following cycles. This may suggest that the first charge/discharge process induces a change from the metastable as-prepared structure to a stable structure that is suitable for repetitive delithiation/lithiation as reported in the case of Li_2FeSiO_4 [57].

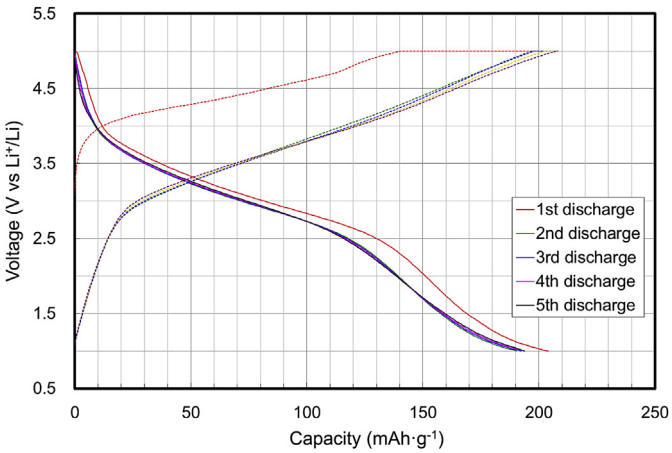

Fig. 1. Charge (solid)/discharge (dotted) curves of the carbon-hybridized Li_2MnSiO_4 particles at the rate of 0.1 C in the range of 1.0–5.0 V at 25 °C.

The laboratory-based and synchrotron-based XRD experiments were performed for the as-prepared, 1st-charged, 1st-discharged, 5th-charged, and 5th-discharged samples in order to understand the structural changes in repetitiously discharged/charged Li_2MnSiO_4, as well as to find the difference in the structure between the as-prepared and the 1st-charged/discharged samples.

The laboratory-based XRD patterns are shown in Fig. 2. Because the measured samples, taken out from a discharged or charged cell, include teflonized acetylene black, the XRD pattern of teflonized acetylene black is also shown in Fig. 2, where diffraction peaks of polytetrafluoroethylene (PTFE) and carbon were identified. The diffraction peaks of the as-prepared sample are indexed with respect to a perfect and long-range, orthorhombic $Pmn2_1(\beta)$ crystal structure of Li_2MnSiO_4. The crystallite size estimated from the full width at the half maximum (FWHM) of the XRD peaks using the Debye–Scherrer formula is about 16 nm, which is in good agreement with the particle size of 10–20 nm observed by transmission electron microscopy (TEM). The TEM observation also reveals that the carbon-hybridized Li_2MnSiO_4 particles consist of Li_2MnSiO_4 nanoparticles surrounded by a carbon phase coating.

After the first-charging, some diffraction peaks disappeared and some diffraction peaks became markedly smaller. But upon the following first-discharging, the missing diffraction peaks reappeared and grew stronger. After the fifth-charging, all diffraction peaks of Li_2MnSiO_4 appeared to vanish completely. However, they reappeared even after the fifth-discharging. Thus the absence of distinct diffraction peaks in the charged (delithiated) structure implies the lack of long-range order crystalline structure in the charged state. The presence of some diffraction peaks in the 1st-charged sample is remarkable, indicating while this sample is partially delithiated into a chemical formula $Li_{0.75}MnSiO_4$ or $1.25MnSiO_4 + 0.75Li_2MnSiO_4$, a part of the β-Li_2MnSiO_4 structure still remains. On the whole, it can be said that samples at the charged state reveal a disordered structure as evident by the absence of diffraction peaks whereas the residual crystalline structure of β-Li_2MnSiO_4 is recovered in the discharged samples.

Fig. 3 shows the synchrotron-based HE-XRD patterns of the same samples. The overall features show more distinct diffraction peaks with better statistics than the laboratory-based XRD patterns. The diffraction peaks indexed to the β-Li_2MnSiO_4 structure account for the same charge/discharge repetitive behavior as those

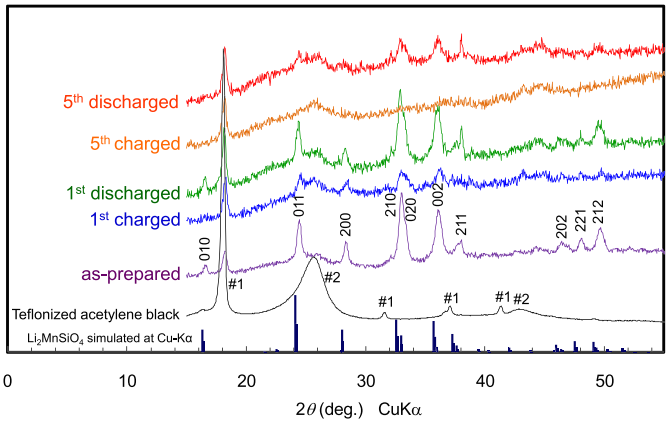

Fig. 2. Laboratory-based XRD patterns of the as-prepared, 1st-charged, 1st-discharged, 5th-charged, 5th-discharged samples, and the teflonized acetylene black. The carbon-hybridized Li_2MnSiO_4 samples were charged or discharged in the delithiation of 1.25 Li/formula-unit. #1 and #2 peaks of teflonized acetylene black correspond to diffraction peaks of PTFE and carbon, respectively. The hkl indices refer to the underlining β-Li_2MnSiO_4 structure.

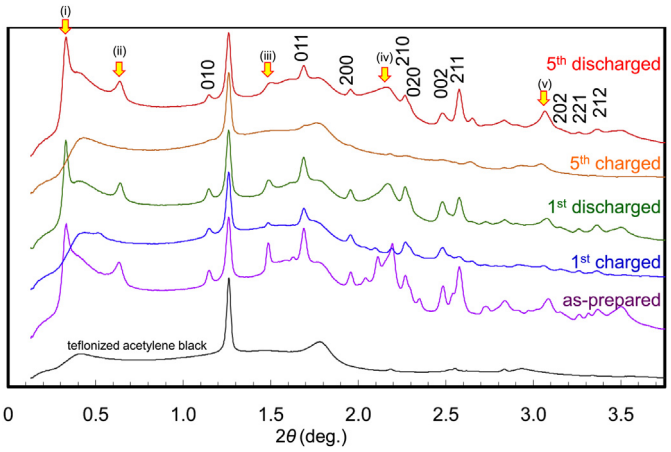

Fig. 3. Synchrotron-based HE-XRD patterns of the as-prepared, 1st-charged, 1st-discharged, 5th-charged, 5th-discharged samples, and the teflonized acetylene black. The carbon-hybridized Li_2MnSiO_4 samples were charged or discharged in the delithiation of 1.25 Li/formula-unit. The hkl indices refer to the underlining β-Li_2MnSiO_4 structure.

revealed the laboratory-based XRD patterns, i.e., the diffraction peaks of β-Li_2MnSiO_4 diminish in the charged samples and reappear in the discharged samples.

Therefore, the delithiated samples may have no long-range order in the structure and the lithiated samples have a long-range order of the β-Li_2MnSiO_4 structure. As shown in Fig. 4, an ideal β-Li_2MnSiO_4 crystallizes in a quasi-layered structure which consists of sheets of alternating corner-sharing MnO_4 and SiO_4 tetrahedra and lithium ions occupying the interlayer tetrahedral sites. A stable lattice structure may be regarded as the result of balancing the electrostatic interactions between the negatively charged MnO_4–SiO_4 layers and the inserted lithium cations. When a portion of the lithium cations are extracted from the space between the MnO_4–SiO_4 layers, a decrease in negative charge of the MnO_4–SiO_4 layers occurs and the electrostatic interaction between the MnO_4–SiO_4 layers and the remaining lithium cations becomes weaker. Thus, the space between the MnO_4–SiO_4 layers may be irregularly altered in the charged samples, resulting in a loss of the long-range order observed in the XRD patterns.

In order to compare the HE-XRD patterns with the laboratory-based XRD patterns we rescaled the 2θ of the HE-XRD, effectively converting $\lambda = 0.1078$ Å to $\lambda = 1.5418$ Å (Cu-Kα). Fig. 5 shows the

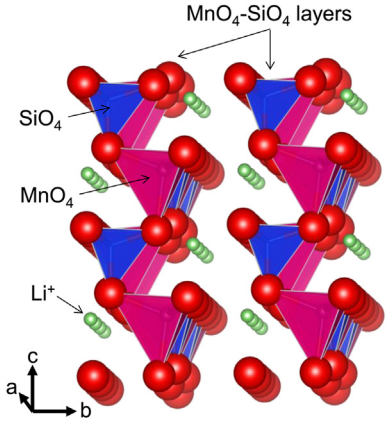

Fig. 4. A schematic crystal structure of $Pmn2_1$ (β) Li_2MnSiO_4. β-Li_2MnSiO_4 is a quasi-layered structure featuring sheets of alternating corner-shared MnO_4 and SiO_4 tetrahedra. Lithium ions occupy the tetrahedral sites between layers.

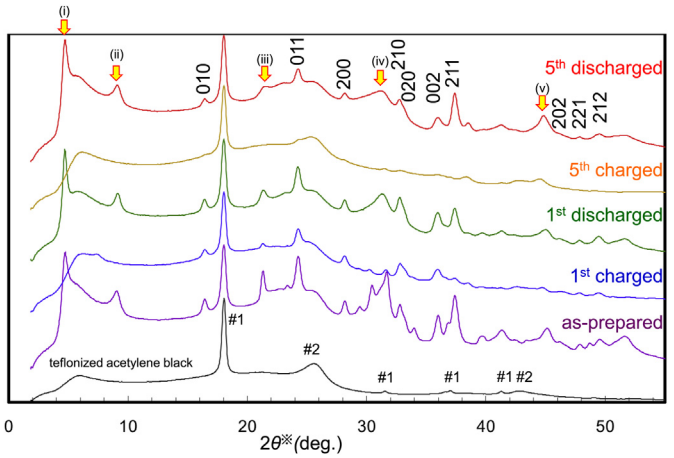

Fig. 5. Converted HE-XRD patterns of the as-prepared, 1st-charged, 1st-discharged, 5th-charged, 5th-discharged samples, and the teflonized acetylene black. 2θ was re-scaled to convert $\lambda = 0.1078$ Å to $\lambda = 1.5418$ Å (Cu-Kα).

converted HE-XRD patterns of the same samples. Some important differences were observed between the corresponding HE-XRD and XRD patterns (Fig. 2). In the HE-XRD patterns, a group of additional peaks denoted by (i), (ii), (iii), (iv), and (v) were superimposed on the diffraction pattern corresponding to the β-Li_2MnSiO_4 structure. These diffraction peaks also show the same behavior as those assigned to β-Li_2MnSiO_4, namely, they disappear in the charged samples and reappear in the discharged samples. Thus, these peaks labeled (i), (ii), (iii), (iv), and (v) must also relate to the change in structure of charged/discharged samples, and the incommensurability of these peaks with respect to the β-Li_2MnSiO_4 structure implies an origin of the disorder structure.

Therefore, the analyses show evidence of a fluctuation between a crystalline structure and a locally disordered structure corresponding directly to the charging (delithiated) and discharging (lithiated) processes in our carbon-hybridized Li_2MnSiO_4 nanoparticles.

By virtue of the high energy – thereby high spatial resolution – of synchrotron X-rays, the local structures of the charged/discharged samples can be investigated by the pair-distribution-function (PDF) analysis. Fig. 6(a) shows the scattering intensities $I(Q)$ as a function of the wave vector Q ($=4\pi\sin\theta/\lambda$) of the same samples and the teflonized acetylene black. Fig. 6(b) shows the corresponding corrected scattering intensities $I(Q)$ by subtracting the background of the teflonized acetylene black.

Fig. 7 shows the $G(r)$, the PDFs in real space, obtained from a Fourier transform of the corrected scattering intensities $I(Q)$ of Fig. 6(b). The merit of this analysis lies in the excellent resolving power at small radial distances, i.e., the local structure, whereas at large distances the features are too complex to interpret quantitatively. Therefore, concentrating on small distances and examining the peaks around 2 Å, we identify a peak at 1.95 Å in the 1st-charged and 5th-charged samples, and in the as-prepared, 1st-discharged, and 5th-discharged samples this same peak shifts to 2.15 Å. This peak around 2 Å is related to spatial correlation of nearest neighbor (n.n.) of Mn–O pairs. Therefore, the mean Mn–O n.n. distance of delithiated samples is shorter than that of the lithiated samples. This is consistent with the notion that smaller Mn^{3+} and Mn^{4+} ions exist in the delithiated samples and lager Mn^{2+} ions in the lithiated counterparts. Thus the change in the peak position around 2 Å corroborates coordinated behavior

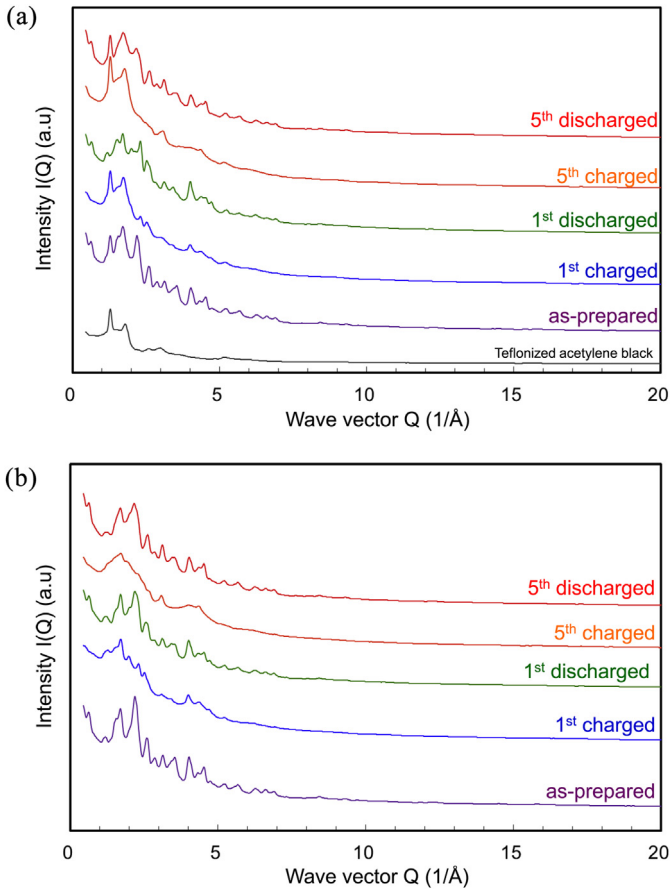

Fig. 6. (a) Scattering intensities $I(Q)$ as a function of the wave vector Q for the as-prepared, 1st-charged, 1st-discharged, 5th-charged, 5th-discharged samples, and the teflonized acetylene black and (b) the corresponding corrected scattering intensities $I(Q)$ by removal of the teflonized acetylene black background.

between the $Mn^{2+}/Mn^{3+}/Mn^{4+}$ valence change and the extraction/insertion of lithium ions.

In the charge/discharge repetition of the carbon-hybridized Li_2MnSiO_4 nanoparticles, the lithiated structure shows a long-range order which dissipates in the delithiated structure. Qualitatively, the long-range structure is evolved to accommodate a local structure characteristic of distorted MnO_4 tetrahedra which

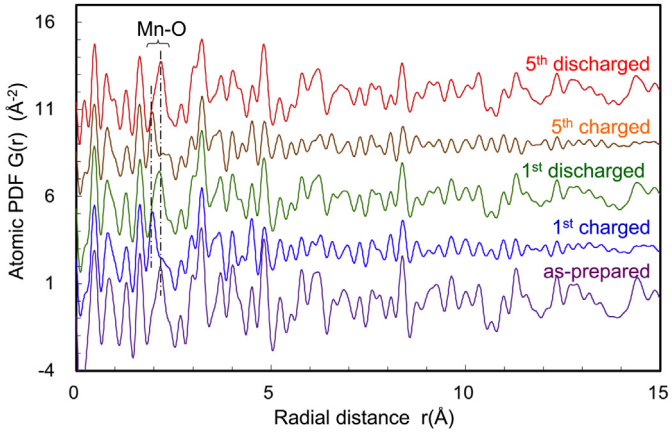

Fig. 7. PDFs $G(r)$ obtained from the corrected scattering intensities $I(Q)$ of Fig. 6(b).

accommodate shorter Mn–O n.n. distances. Furthermore, the shorter Mn–O distance corresponds to the smaller Mn^{3+} and Mn^{4+} ions in the delithiated samples. Upon charging (lithiation) the long-range order recovers. Our analysis shows that such structure fluctuation, apparently only occurring in the carbon-hybridized Li_2MnSiO_4 nanoparticles, allows the extraction/insertion of the lithium ions in the interlayer sites yet maintaining the overall stable structure of the material.

We now remark on the observation of a different charge/discharge behavior only in the first charge/discharge cycle (see Fig. 1). However, no drastic change was observed in XRD, HE-XRD, and PDF between the as-prepared and 1st-, 5th-discharged samples. The basic local structure and long-range ordered structure are unchanged by the first charge/discharge but the potential of the first charge/discharge is higher than those of other cycled charges/discharges. This means that a higher potential is needed for the first extraction/insertion of lithium ions, and in subsequent extraction/insertion of lithium ions a lower potential suffices. One conjectures would be that the first charge/discharge with a high potential may effect a change on the surface of Li_2MnSiO_4 nanoparticles, for example by forming a solid electrolyte interface (SEI).

4. Conclusions

We have prepared carbon-hybridized Li_2MnSiO_4 nanoparticles by a novel synthesis using spray pyrolysis of a precursor solution with glucose as a carbon source. This material exhibits excellent charge/discharge cycling durability with a high capacity about 190 mAh g^{-1} corresponding to a lithiation of about 1.15 Li ion per formula unit. The charged/discharged structures in the carbon-hybridized Li_2MnSiO_4 nanoparticles have been studied by laboratory-based XRD, synchrotron-based HE-XRD, and the combined results analyzed by crystal structure and PDF analyses. The discharged samples show a long-range ordered structure that dissipates in the charged samples. However, each discharging process recovers the long-range order. In other words, the repetitive disappearance/reappearance of the long-range order fully correlates with the charge/discharge cycling. The disappearance of the long-range order is caused by a local structure that accommodates distortions of the MnO_4 tetrahedra. The mean Mn–O n.n. distance of the charged structure is shorter than the corresponding Mn–O distance of the discharged crystalline structure, a finding corroborating the notion of the change in the $Mn^{2+}/Mn^{3+}/Mn^{4+}$ ionic radius with respect to the extraction/insertion of lithium ions.

Only the first charge/discharge cycle requires a potential higher than that of all subsequent cycles but no change was observed in XRD, HE-XRD patterns, nor in the PDF results. This implies that if a structural change effects a high potential required in the first charge/discharge, it is not related to the locally disordered or long-rage ordered structures of Li_2MnSiO_4 but rather to an electrochemical change due to a microstructural modification of the carbon-phase in Li_2MnSiO_4 nanoparticles.

Acknowledgments

Use of the Advanced Photon Source, an Office of Science User Facility operated for the U.S. Department of Energy (DOE) Office of Science by Argonne National Laboratory, was supported by the U.S. DOE under Contract No. DE-AC02-06CH11357. We greatly appreciate Dr. Chun-K. Loong, who has given us the opportunity to measure the synchrotron-based XRD and the helpful comments.

References

[1] R. Dominko, M. Bele, M. Gaberscek, A. Meden, M. Remskar, J. Jamnik, Electrochem. Commun. 8 (2006) 217.
[2] R. Dominko, I. Arcon, A. Kodre, D. Hanzel, M. Gaberscek, J. Power Sources 189 (2009) 51.
[3] M.E. Arroyo-de Dompablo, M. Armand, J.M. Tarascon, U. Amader, Electrochem. Commun. 8 (2006) 1292.
[4] S.Q. Wu, Z.Z. Zhu, Y. Yang, Z.F. Hou, Comput. Mater. Sci. 44 (2009) 1243.
[5] B. Xu, D. Qian, Z. Wang, Y.S. Meng, Mater. Sci. Eng. R 73 (2012) 51.
[6] R.C. Longo, K. Xiong, K. Cho, J. Electrochem. Soc. 160 (2013) A60.
[7] K. Zaghib, A.A. Salah, N. Ravet, A. Mauger, F. Gendron, C.,M. Julien, J. Power Sources 160 (2006) 1381.
[8] A. Nyten, M. Stjerndahl, H. Rensmo, H. Siegbahn, M. Armand, T. Gustafsson, K. Edstrom, J.O. Thomas, J. Mater. Chem. 16 (2006) 3483.
[9] S. Nishimura, S. Hayase, R. Kanno, M. Yashima, N. Nakayama, A. Yamada, J. Am. Chem. Soc. 130 (2008) 13212.
[10] R. Dominko, D.E. Conte, D. Hanzel, M. Gaberscek, J. Jamnik, J. Power Sources 178 (2008) 842.
[11] M. Nadherna, R. Dominko, D. Hanzel, J. Roiter, M. Gaberscek, J. Electrochem. Soc. 156 (2009) A619.
[12] R. Domimko, C. Sirisopanaporn, C. Masquelier, D. Hanzel, I. Arcon, M. Gaberscek, J. Electrochem. Soc. 157 (2010) A1309.
[13] D. Lv, W. Wen, X. Huang, J. Bai, J. Mi, S. Wu, Y. Yang, J. Mater. Chem. 21 (2011) 9506.
[14] C. Sirisopanaporn, R. Dominko, C. Masquelier, A.R. Armstrong, G. Mali, P.G. Bruce, J. Mater. Chem. 21 (2011) 17823.
[15] C. Sirisopanaporn, C. Mesqueller, P.G. Bruce, A.R. Armstrong, R. Dominko, J. Am. Chem. Soc. 133 (2011) 1263.
[16] C. Sirsopanaporn, C. Masquerlier, P.G. Bruce, A.R. Armstrong, R. Dominko, J. Am. Chem. Soc. 133 (2011) 1263.
[17] N. Yabuuchi, Y. Yamakawa, K. Yoshiii, S. Komaba, Dalton Trans. 40 (2011) 1846.
[18] G. Mali, C. Sirisopanaporn, C. Masquerlier, D. Hanzel, R. Dominko, Chem. Mater. 23 (2011) 2735.
[19] A.R. Armstrong, N. Kuganathan, M.S. Islam, P.G. Bruce, J. Am. Chem. Soc. 133 (2011) 13031.
[20] C. Deng, S. Zhang, S.Y. Yang, B.L. Fu, L. Ma, J. Power Sources 196 (2011) 386.
[21] T. Kojima, A. Kojima, T. Miyuki, Y. Okuyama, T. Sakai, J. Electrochem. Soc. 158 (2011) A1340.
[22] C. Eames, A.R. Armstrong, P.G. Bruce, M. Islam, Chem. Mater. 24 (2012) 2155.
[23] Y. Li, X. Cheng, Y. Zhang, J. Electrochem. Soc. 159 (2012) A69.
[24] A. Kojima, T. Kojima, M. Tabuchi, T. Sakai, J. Electrochem. Soc. 159 (2012) A725.
[25] Z. Yan, S. Cai, X. Zhou, Y. Zhao, L. Miao, J. Electrochem. Soc. 159 (2012) A894.
[26] R. Fu, Y. Li, H. Yang, Y. Zhang, X. Cheng, J. Electrochem. Soc. 160 (2013) A3048.
[27] Y. Li, Z. Gong, Y. Yang, J. Power Sources 174 (2007) 528.
[28] A. Kokalj, R. Dominko, G. Mali, A. Meden, M. Gaberscek, J. Jamnik, Chem. Mater. 19 (2007) 3633.
[29] V.V. Politaev, A.A. Petrenko, V.B. Nalbandyan, B.S. Medvedev, E.S. Shvetsova, J. Solid State Chem. 180 (2007) 1045.
[30] M.E. Arroyo-de Dompablo, R. Dominko, J.M. Gallardo-Amores, L. Dupont, G. Mali, H. Ehrenberg, J. Jamnik, E. Moran, Chem. Mater. 20 (2008) 5574.
[31] W. Liu, Y. Xu, R. Yang, J. Alloys Compd. 480 (2009) L1.
[32] P. Ghosh, S. Mahanty, R.N. Basu, J. Electrochem. Soc. 156 (2009) A677.
[33] T. Muraliganth, K.R. Stroukoff, A. Manthiram, Chem. Mater. 22 (2010) 5754.
[34] C. Deng, S. Zhang, B.L. Fu, S.Y. Yang, L. Ma, Mater. Chem. Phys. 120 (2010) 14.
[35] H. Duncan, A. Kondamreddy, P.H.J. Mercier, Y.L. Page, Y. Abu-Lebdeh, M. Couillard, P.S. Whitfield, I.J. Davidson, Chem. Mater. 23 (2011) 5446.
[36] V. Aravindan, K. Karthikeyan, K.S. Kang, W.S. Yoon, W.S. Kim, Y.S. Lee, J. Mater. Chem. 21 (2011) 2470.
[37] V. Aravindan, S. Ravi, W.S. Kim, S.Y. Lee, Y.S. Lee, J. Colloid Interface Sci. 355 (2011) 472.
[38] X. Kong, T. Mei, Z. Xing, N. Li, Z. Yuan, Y. Zhu, Y. Qian, Int. J. Electrochem. Sci. 7 (2012) 5565.
[39] C. Deng, Y.H. Sun, S. Zhang, H.M. Lin, Y. Gao, B. Wu, L. Ma, Y. Shang, G. Dong, Int. J. Electrochem. Sci. 7 (2012) 4559.
[40] K. Karthikeyan, S. Amaresh, J.N. Son, Y.S. Lee, J. Electrochem. Sci. Technol. 3 (2012) 72.
[41] A. Bhaskar, M. Deepa, T.N. Rao, U.V. Varadaraju, J. Electrochem. Soc. 159 (2012) A1954.
[42] A. Kojima, T. Kojima, M. Tabuchi, T. Sakai, J. Electrochem. Soc. 159 (2012) A532.
[43] S. Devaraj, M. Kuezma, C.T. Ng, P. Balaya, Electrochim. Acta 102 (2013) 290.
[44] B. Shao, Y. Abe, I. Taniguchi, Powder Technol. 235 (2013) 1.
[45] F. Wang, J. Chen, C. Wang, B. Yi, J. Electroanal. Chem. 688 (2013) 123.
[46] J. Liu, H. Xu, X. Jiang, Y. Qian, J. Power Sources 231 (2013) 39.
[47] S. Liu, J. Xu, D. Li, Y. Hu, X. Liu, K. Xie, J. Power Sources 232 (2013) 258.
[48] D. Sun, H. Wang, P. Ding, N. Zhou, X. Huang, S. Tan, Y. Tang, J. Power Sources 242 (2013) 865.
[49] X. Jiang, H. Xu, J. Liu, Y. Qian, Mater. Lett. 113 (2013) 9.

[50] M. Swietosiawski, M. Moienda, K. Furczon, R. Dziembaj, J. Power Sources 244 (2013) 510.
[51] H. Wang, T. Hou, D. Sun, X. Huang, H. He, Y. Tang, Y. Liu, J. Power Sources 247 (2014) 497.
[52] X. Li, Y. Liu, Z. Xiao, W. Guo, R. Zhang, Ceram. Int. 40 (2014) 289.
[53] H. Gong, Y. Zhu, L. Wang, D. Wei, J. Liang, Y. Qian, J. Power Sources 246 (2014) 192.
[54] F. Wang, Y. Wang, D. Sun, L. Wang, J. Yang, H. Jia, Electrochim. Acta 119 (2014) 131.
[55] L. Qu, S. Fang, L. Yang, S. Hirano, J. Power Sources 252 (2014) 169.
[56] M. Moriya, M. Miyahara, M. Hokazono, H. Sasaki, A. Nemoto, S. Katayama, Y. Akimoto, S. Hirano, J. Electrochem. Soc. 161 (2014) A97.
[57] A. Kojima, T. Kojima, T. Sakai, J. Electrochem. Soc. 159 (2012) A525.